RESEARCH PAPER

Creep and ageing of granular materials under isotropic pressure

Belinda Anna-Maria Jessen[1] · Roberto Cudmani[1] · Stefan Vogt[1]

Abstract

Single- and multi-stage isotropic creep tests including bender element and acoustic emission measurements are carried out to investigate the relationship between ageing and creep in dense silica sand. In the considered pressure range, the experimental results show an inversely proportional relationship between ageing and creep: the small-strain shear modulus increases with decreasing isotropic pressure,, while the axial creep strain and the acoustic emissions show the opposite pressure dependence. In the multi-stage creep test, the small-strain shear modulus increases monotonically, while the rates of axial strain, number of acoustic emissions and small-strain shear modulus decrease with time according to a power law. In the single-stage creep tests, the ageing and creep indicators initially evolve as in the multi-stage creep test, but then the small-strain shear modulus reaches a peak value and decreases with time thereafter. At the same time, the rates of axial strain, number of acoustic emissions and small-strain shear modulus deviate from the power law. A conceptual model assuming a time-dependent behaviour of the normal and shear forces at the particle contacts in order to explain the experimental observations qualitatively is proposed. Accordingly, an increase in small-strain shear modulus results from homogenisation of the force chains, while a decrease in small-strain shear modulus results from a temporary formation followed by a time-delayed collapse of strong force chains.

Keywords Acoustic emissions · Ageing · Creep · Granular assembly · Particle contact · Silica sand

List of symbols

A	Observation area of particle roughness determination
a	Inclination of the Gutenberg–Richter law
AE	Acoustic emission
b	Intercept with the ordinate of the Gutenberg–Richter law
BE	Bender elements
C_C	Coefficient of gradation
C_U	Uniformity coefficient
CPT	Cone penetration testing
D	Duration of an AE event
$D_{r,0}$	Initial relative density of a sample
d_{50}	Mean particle diameter
E	Signal burst energy of an AE event
E_{max}	Maximum accumulated signal burst energy
e_{max}	Maximum void ratio
e_{min}	Minimum void ratio
ε_a	Axial strain
$\dot{\varepsilon}_a$	Rate of axial strain
$\dot{\varepsilon}_r$	Rate of radial strain
G_0	Small-strain shear modulus
$G_{0,t}$	Small-strain shear modulus at time t
$\Delta G_{0,t}$	Change in the small-strain shear modulus at time t
$\dot{G}_{0,t}/G_{0,t=0}$	Rate of change of small-strain shear modulus at time t normalised to the shear modulus at $t = 0$ s.
m	Exponent describing a power law
M	Magnitude of a seismic event
N	Number of seismic events
N_{AE}	Number of AE events
$\dot{N}_{AE}$	Rate of number of AE events
$N_{AE,max}$	Maximum accumulated number of AE events
p'	Effective mean pressure
R	Particle roundness

✉ Belinda Anna-Maria Jessen
belinda.jessen@tum.de

Roberto Cudmani
r.cudmani@tum.de

Stefan Vogt
s.vogt@tum.de

1 TUM School of Engineering and Design, Department of Civil and Environmental Engineering, Technical University of Munich, Munich, Germany

ρ	Density of the sample
ρ_s	Particle density
S	Particle sphericity
S_q	Particle roughness
$\dot{\sigma}_a$	Rate of axial pressure
$\dot{\sigma}_r$	Rate of radial pressure
$u(t)$	Time-dependent signal voltage of an AE event
v_s	Shear wave velocity

1 Introduction

Young granular soils deposited by natural or anthropogenic processes and granular soils that lost their natural structure by construction processes such as pile driving or soil compaction by vibration, change their mechanical properties within readily observable time scales. This time-dependent process is also referred to as ageing [26]. Examples highlighting the ageing of sand regarding mechanical properties such as strength and stiffness are the increasing bearing capacity of piles posterior to their installation [8, 10, 34], the increasing resistance measured by cone penetration tests (CPT) in fills [27, 32] as well as the increasing shear modulus at small strain [1, 2]. At constant effective pressure, density changes occur by time; this process is called creep. In contrast to fine-grained soils creep in granular soils is less pronounced [3], however, for certain geotechnical challenges time-dependent deformation has to be taken into account. Examples are open cast mining dumps with thicknesses up to several hundreds of metres [9, 22] or foundations of buildings and infrastructure on backfilled layers of sands that were compacted by vibro-pressure methods [11].

The time-dependent phenomena of creep and ageing occur simultaneously, whereas a relationship between the corresponding measurable quantities, i.e. the strain rate during creep and stiffness changes, is expected. By experiments, various researchers have investigated the creep and/or ageing behaviour of different sands, e.g. [4, 7, 12, 29, 40], but without presenting a comparative analysis and furthermore an explanation considering the interaction between the two phenomena, which is the objective of the present work.

Schmertmann [32] concluded that primarily micromechanical processes, which take place during creep, are the main cause of ageing. Surface abrasion of particles, formation of microcracks, and different degrees/intensities of particle breakage are fundamental processes during creep,

especially at considerable high pressure [14, 24]. Furthermore, particle translation and rotation, which occur time-dependently at constant pressure, change the arrangement of the particles, as well as the formation of particle contacts [18, 20]. In granular materials, load transfer occurs inhomogeneously considering the so-called meso-scale, which considers individual particles in a particle assembly (equivalent term: grain skeleton). A distinction is made between particles that are part of force chains carrying comparatively large forces and the surrounding low-loaded particles [31]. The aforementioned time-dependent micromechanical processes can cause lateral deflection (alternatively termed as "buckling") of the heavily loaded force chains [7, 19]. Thus, the mechanisms during creep cause a rearrangement of force chains including a restructuring of the particle contacts resulting in a stiffer particle assembly [7, 41]. The comparably small change of density of granular materials during creep can merely explain the increase of the shear modulus G_0 at small strain (i.e. $< 10^{-5}$) with time [1].

Furthermore, the sliding resistance between particles increases by the rise of interlocking effects considering the particle surface at the individual particle contacts, sometimes referred to as "micro interlocking" [23]. By experimental studies observing the behaviour of loaded individual particles at the micro-scale Michalowski et al. [25] identify processes termed as "contact maturing". The contact maturing describes the "improvement" and therefore stiffness increase in particle contacts linked to time-dependent changes of the particle morphology resulting from abrasion of the surface texture and breakage of particle asperities and is seen as a further cause of macroscopically observable ageing effects.

In this paper, a combined experimental study on creep and ageing of granular materials is presented. The macroscopic ageing effects are quantified through the evolution of the small-strain shear modulus $G_{0,t}$ during creep under constant pressure. $G_{0,t}$ is determined from shear wave velocity measured by piezo-electric bender elements. The experimental investigation is carried out on natural silica sand. The acoustic emission method is used to quantify the micromechanical mechanisms between individual particles that occur during creep or lead to ageing. The dependence on the effective pressure and the influence of the stress–strain history are investigated by so-called single- and multi-stage creep tests. The single-stage creep test consists of one creep phase after isotropic compression whereas during the multi-stage creep test at least one phase of creep was observed after a creep phase was conducted at lower pressures. The effective pressures kept constant during creep range between 500 and 2000 kPa. This range corresponds to rather common geotechnical boundary-value

problems such as dumped soil by earthworks or mining activities, compacted soil, cone penetration testing (CPT) and pile foundation. For silica sand even at a pressure of 2000 kPa it is assumed that intense particle breakage is not decisive during creep and the processes at the particle contact are mainly governed by the abrasion of the particle surface and the minor intensity of the breakage of particle asperities. Based on the experimental findings, a conceptual model is proposed to explain the evolution of soil structure during ageing and creep qualitatively.

2 Material and methods

2.1 Material

Silica sand, taken from a sand quarry at Midlum located on a so-called geest formed by glacial loadings near to the city of Cuxhaven, Germany, was used for the investigation. The Cuxhaven sand is of predominately quartz SiO_2 (95 wt%), which contains traces of albite (3 wt%) and K-feldspar (2 wt%). The particle size distribution of the uniform and well-graded material is shown in Fig. 1. The granular properties are given in Table 1.

The roundness R and sphericity S were determined according to the definition of Krumbein and Sloss [17]. These particle shape parameters as well as the particle size distribution were determined by dynamic image analysis
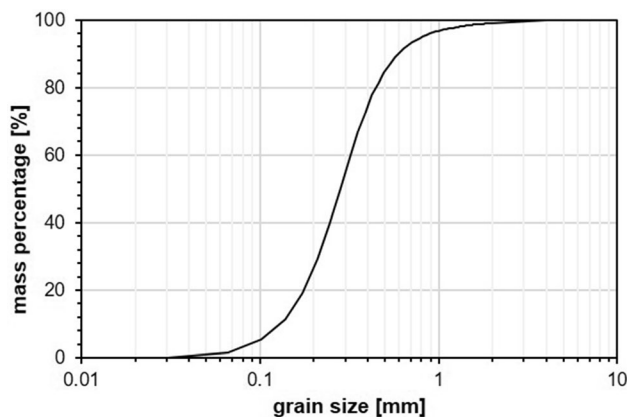

Fig. 1 Particle size distribution of Cuxhaven sand

taken by a laser-scanning optical device. The roughness, measured by a laser-scanning confocal microscope, is described by the two-dimensional parameter S_q [13] as follows

$$S_q = \sqrt{\frac{1}{A} \iint_A z^2(x,y) \mathrm{d}x \mathrm{d}y^2}, \tag{1}$$

where A describes the area of observation and z the height of the surface at position x and y according to a reference coordinate system chosen by the user. For a meaningful particle shape analysis in context to the given problem, the definition of a low-pass filter is necessary. The area of contact between two silica sand particles of Ottawa sand at a grain size between 0.60 and 0.84 mm was illustrated by Michalowski et al. [25]. They showed that asperity breakage occurs at a scale of 10 μm. Hence, for our microscopy, a Gauss cut-off filter of 10 μm was selected to evaluate the roughness in a defined area of observation of $A = 500$ μm^2. In Fig. 2, images of the particle shape and surface texture of Cuxhaven sand are given.

According to the determined granular properties, Cuxhaven sand is uniformly graded with an angular to round particle shape and a comparably small surface roughness related to the scale of particle contacts.

2.2 Triaxial test setup and conventional measurement

For conducting the isotropic compression und subsequently following creep phases, we used a setup of two triaxial apparatus. Figure 3 shows a photography of one triaxial apparatus and a schematic sketch of the triaxial cell including the main components. A device with electromechanical ball screw drives for pressure control was used to apply the isotropic pressure on the sample. Test control, data acquisition and visualisation during the test were automatized. The resolution of the measured pressure is given by 0.1 kPa. In addition to the cell pressure, the specimen was subjected to a small axial force applied by the loading ram penetrating into the pressure cell to ensure specimen contact, which was necessary to measure the change of the axial deformation of the specimen. The measurement of the axial deformation of the sample
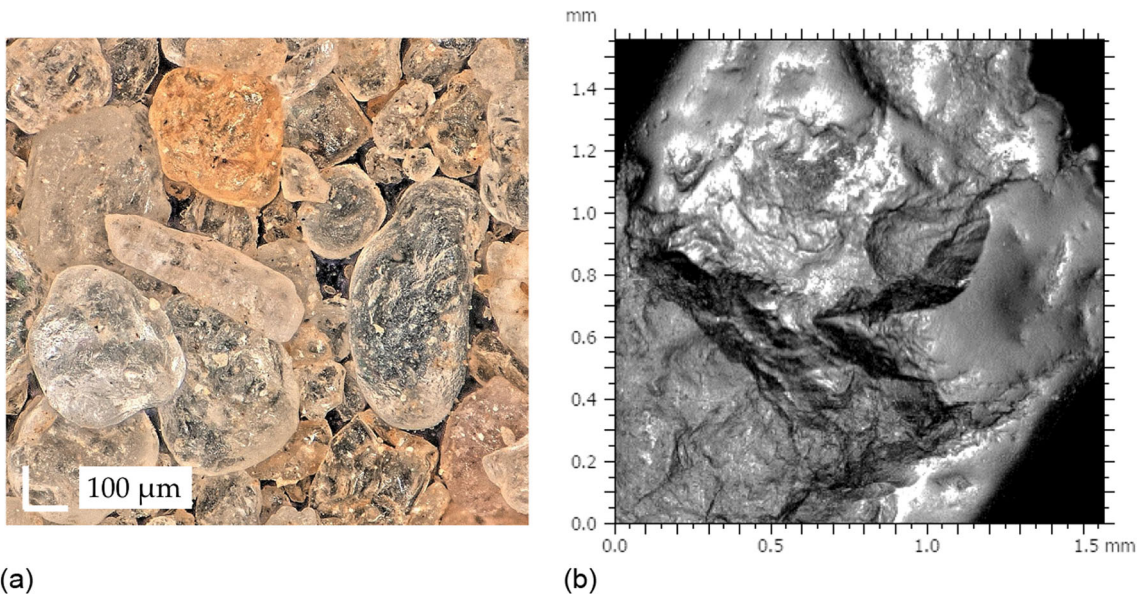
Table 1 Granular properties of Cuxhaven sand

Particle density and strength		Limiting void ratios		Particle size distribution			Particle shape		
ρ_s[g/m^3]	Mohs hardness	e_{max}	e_{min}	d_{50}[mm]	C_U	C_C	R	S	S_q[μm]
2.62	6.0 to 7.0	0.75	0.48	0.29	2.62	1.14	0.54	0.77	0.32

Fig. 2 Images illustrating **a** the particle shape; **b** the surface texture of Cuxhaven sand
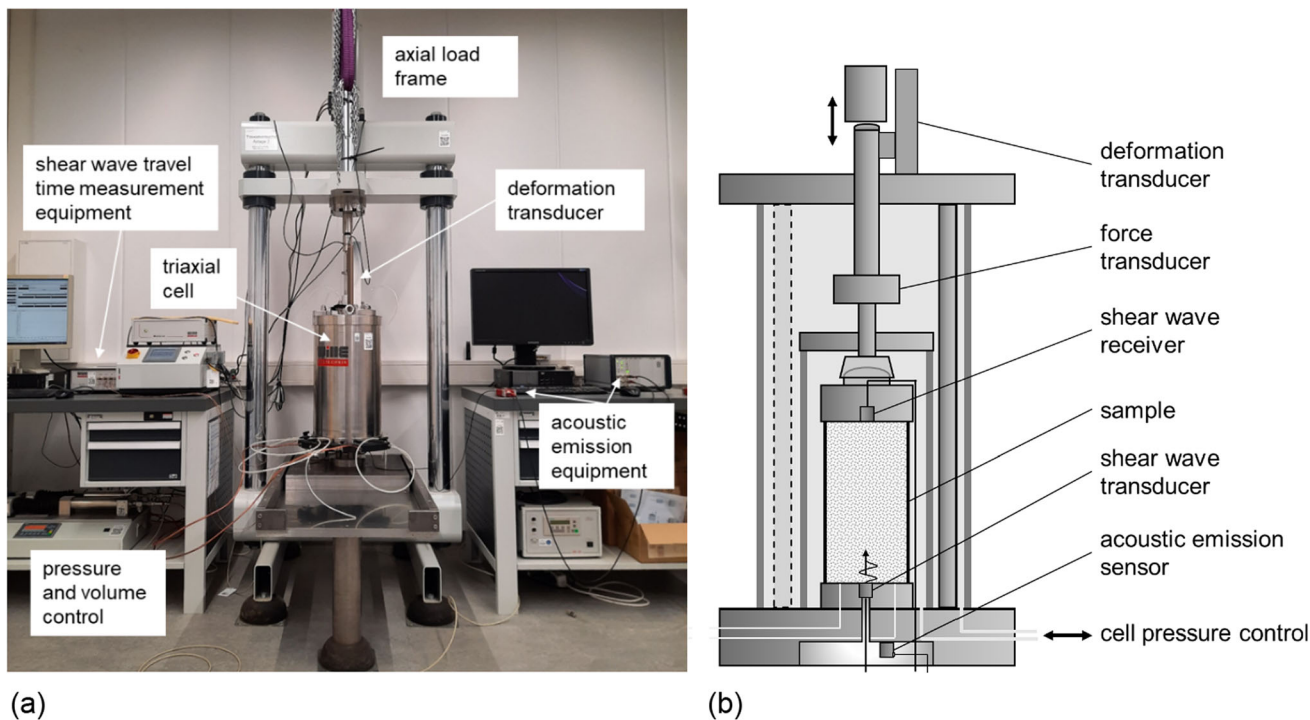

Fig. 3 **a** Photography of the triaxial test setup; **b** Schematic sketch of the triaxial cell comprising the main components for the measuring system

comprises a linear encoder owing a resolution of 0.025 μm. The accuracy of the sensor is specified as ± 5 μm/m. The load frame comprises an electromechanical ball screw drive with a nominal force of 100 kN. During the creep phases, the isotropic pressure on the soil sample was kept constant with an accuracy of < 0.14% with respect to the nominal value calibrated by traceable measuring equipment.

2.3 Testing procedure

Creep and ageing of dense to very dense samples of Cuxhaven sand were investigated under isotropic compression. During the tests, acoustic emissions were continuously recorded. To investigate the influence of previous creep phases on the posterior creep and ageing of the samples, the two test procedures illustrated schematically
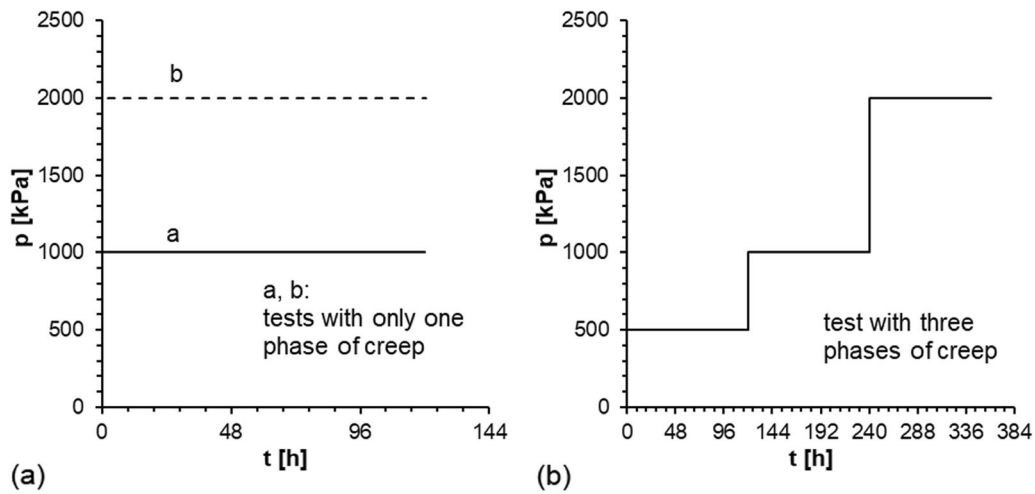
Fig. 4 Test procedure of **a** single-stage creep test; **b** multi-stage creep test with first phase of creep considered as single-stage creep

Table 2 Prescribed and measured pressure and strain rates for phases of isotropic loading and creep phases during the test procedure

Phase	Variable	Prescribed condition	Measured values
Loading	Axial and radial pressure rate	$\dot{\sigma}_a = \dot{\sigma}_r = 100$ kPa/min	
	Axial and radial strain rate		$\dot{\varepsilon}_a = \dot{\varepsilon}_r \neq 0$
Creep	Axial and radial pressure rate	$\dot{\sigma}_a = \dot{\sigma}_r = 0$	
	Axial and radial strain rate		$\dot{\varepsilon}_a = \dot{\varepsilon}_r \neq 0$

in Fig. 4 were used. For the single-stage creep tests, different samples were loaded by a constant isotropic loading rate of 100 kPa/min up to an effective mean pressure of $p\prime = 1000$ kPa and 2000 kPa, respectively. The following creep phase lasted up to at least five days. To conduct the multi-stage creep phases, a sample was loaded with the same constant isotropic loading rate of 100 kPa/min up to $p\prime = 500$ kPa at which the first phase of creep was observed. As well this phase of creep lasted until at least five days. Subsequently, the pressure was increased to $p\prime = 1000$ kPa at a rate of 100 kPa/min and a second creep phase for another five days was implemented. Finally, the procedure was repeated for a third creep phase at an isotropic pressure of $p\prime = 2000$ kPa. The first phase of creep of the test is evaluated as a single-stage creep phase, while the second and third creep phases represent multi-stage creep phases.

Either pressure or strain rates are controlled by the triaxial apparatus in each of the test phases. The test procedures are summarised in Tab.2.

For simplicity, only the axial strain ε_a evolving during creep is presented in this study.

2.4 Shear wave travel time measurements

The shear modulus at small-strain G_0 for the magnitudes of $\gamma \leq 10^{-5}$ was determined by

$$G_0 = \rho \cdot v_s^2, \tag{2}$$

where ρ is the actual density of the sample for the time at which the shear wave velocity v_s was measured. The shear wave velocity v_s was calculated from the measured travel time of the shear wave through the sample in axial direction.

Conventional bender elements (BE) made of piezo-ceramic were used for initiating (actuator) and measuring (sensor) the wave. The wave actuator was connected to a waveform generator that provides a burst signal in form of a sine wave, leading the bending of the piezo-ceramic plates. The excitation frequency was selected regarding the mechanical resonance frequency of the sensor which was given by the manufacturer at 5 kHz. The shear wave propagated through the sample and was recorded by the receiver. An oscilloscope amplified and visualised the incoming signal. The evaluation of the shear wave travel time in order to calculate v_s to be used in Eq. (2) was done by the so-called start-to-start method, which was found to be the most robust in our study.

To determine the ageing of the sample during the creep phases, the change of the small-strain shear modulus $\Delta G_{0,t}$ was determined at certain times t during the creep phase. By setting $t = 0$ s at the beginning of a creep phase once the target value of the effective mean pressure $p\prime$ was reached, the measurement of shear modulus at small strains

$G_{0,t}$ was performed at approximately $t \approx 0$ s, 60 s, 120 s, 300 s and subsequent doubling the measurement intervals. The change of G_0 was evaluated using the time corresponding to the second zero crossing of the incoming signal. The second zero crossing was used for the evaluation because it was well observed over the entire test series compared to the first zero crossing. The method to determine the change of the shear wave travel time during creep is described in detail in Bock et al. [6]. The change of the shear modulus at small strains $\Delta G_{0,t}$ at the time t in relation to the absolute value $G_{0,t=0}$ at $t = 0$ s was considered to result from ageing. Using this method, the waves are assumed to propagate between transmitter and receiver through an ideally homogeneous continuum. We mention that an inhomogeneous particle assembly and hence varying contact forces as well as locally changing density especially in the near field of the transmitter and receiver influences the measurements.

2.5 Acoustic emission measurement

The acoustic emission measurement was performed to provide an insight to the processes at the micro- and mesoscale, e.g. those resulting from mechanisms at the contact between particles and particle clusters. The measurements were carried out and analysed during the creep phases. Acoustic emissions are elastic waves generated by the sudden release of kinetic energy of materials that have previously accumulated elastic energy according to ageing, temperature gradients or mechanical loading. The vibrations can be converted into electrical signals by piezo-electric sensors. The method has already been used in granular materials for monitoring stability of slopes [16, 33, 36] as well as for studying the micromechanical processes during shearing and compression of granular materials in the laboratory [5, 15, 30, 35].

The measurement setup consists of a sensor, preamplifier, signal processor and a visualising software, which also enables the data post-processing. The sensor with a sensitivity range of 20–450 kHz was placed directly at the base plate of the triaxial cell below the sample, see Fig. 3. A detailed description of the measurement system and

Table 3 Settings of acoustic emission measurement

Setting	Used value
Pre-amplification	34 dB
Sampling rate	10 MHz
Digital band-pass filter	25 kHz to 300 kHz
Threshold	45 dB
Rearm time = duration discrimination time	204.8 μs

settings is given in Bock et al. [5]. Table 3 summarises the parameters chosen for the acoustic emission measurement in the triaxial test setup. The threshold describes the minimum amplitude at which a signal was identified as an acoustic emission event (AE-event). This threshold value, which was determined by pretests with a solid dummy made out of PTFE, corresponds to the amplitude at which no acoustic emissions are detected at constant pressure.

The number of AE-events N_{AE} was counted during each creep phase. In addition to N_{AE}, the so-called burst signal energy E was evaluated according to Eq. (3).

$$E = \int_D u^2(t)\mathrm{d}t, \qquad (3)$$

where D is the burst signal duration defined as the time between the first and the last threshold crossing and $u(t)$ the time-dependent signal voltage of the burst signal. The burst signal energy E has a unit of 1 eu that corresponds to 10^{-14} Vs^2. Using a defined reference resistance of 10 kOhm, 1 eu can be scaled to 10^{-18} J. The burst signal energy E is a measure of the released kinetic energy related to the motion of the particles and vanishes when internal and external forces are in a static equilibrium, i.e. the particles are in repose.

2.6 Sample preparation

The absolute axial creep strain and strain rates of granular materials are quite small compared to the strains and strain rates occurring in soft fine-grained and organic soils where the consideration of creep is essential to describe comprehensively the mechanical behaviour. To improve the measurability of strain changes during creep, samples with a comparably high initial specimen height of 200 mm and an initial specimen diameter of 100 mm were used. The samples were prepared by air pluviation. This method allows producing relatively uniform and reproducible samples, showing a fabric that is close to naturally deposited sand [28, 38]. The sand was pluviated by a sand rainer into a multi-part specimen mould, at which the membrane for the triaxial test was wrapped along the inner surface of the cylindrical mould. The basic design of the sand rainer consists of a container that can be opened by a shutter. Depending on the porosity of the opening through perforated plates, which controls the rate of deposition and deposition intensity, respectively, the sand falls in streams onto the so-called diffuser consisting of two sieves arranged at an angle of 45° to each other. The diffuser distributes the particles homogeneously over the section. The falling height, defined by the difference in length between the lowest diffusor sieve and the sample surface, varies during the process of pluviation because an apparatus with

fixed diffusor sieves was used. Vaid and Negussey [38] found that a terminal velocity is reached at a certain falling height depending on the material. With this assumption, a minimum falling height was chosen that exceeded the critical height. Using a perforated plate with a porosity of 3%, dense to very dense samples (relative density $D_r = 0.80$–0.91) were produced. The initial density was determined by measuring the sample dimensions after removing the specimen mould. An initial vacuum providing an effective mean pressure of approximately $p\prime = 20$ kPa stabilised the sample until it was loaded by a cell pressure of $p\prime = 50$ kPa.

3 Experimental results

In the following, the results of the single-stage and multi-stage creep tests are presented for dense to very dense samples of Cuxhaven sand. The main measured quantities within the scope of this study are the axial strain, the change of the small-strain shear modulus and acoustic emissions during creep phases.

The curves that show the data measured during the single-stage creep phases are given in black colour and the results of the multi-stage creep phases are highlighted by grey colour. For concise presentation of the results, in addition to the linear representation over time the logarithmic representation is chosen. Figure 5 shows the axial creep strains (a) with time and (b) as a function of the logarithm of time. The experiments on Cuxhaven sand show that the axial strain ε_a during creep increases with isotropic pressure, as it was already observed by other researchers, e.g. [19], 21. Single-stage creep tests show a higher axial creep strain compared to creep phases of

multi-stage creep tests at similar creep pressures. Regarding the behaviour in the $\log(t) - \varepsilon_a$ – diagram, the results from the single-stage creep tests show a changing slope with time after approximately 10,000 s, which is not evident for multi-stage creep.

The change of the shear modulus $\Delta G_{0,t}$ with time t during creep normalised in respect to the measured absolute value $G_{0,t=0}$ as a function of t and of $\log(t)$ is shown in Fig. 6a, respectively b. Cuxhaven sand shows for all experiments a linear increase of $\Delta G_{0,t}/G_{0,t=0}$ with $\log(t)$ between 60 s and approximately 10,000 s. Afterwards $\Delta G_{0,t}/G_{0,t=0}$ reduced with increasing time for the single-stage creep tests, while the shear modulus measured in phases of creep that where conducted after a previous creep phase do not show any decrease within the period of 5 days. As can be seen in Fig. 6b, ageing, defined as $\Delta G_{0,t}/G_{0,t=0}$, increases with decreasing pressure. Furthermore, the higher the pressure, the more pronounced is the decrease of the shear modulus and the faster the turning point is achieved in the single-stage creep tests.

Figure 7a presents the accumulated number of AE-events N_{AE} evolving linear with time. The number of AE-events for samples of Cuxhaven sand increases with pressure; the pressure-dependence is significant. Thus, for better comparison of the general behaviour, N_{AE} was normalised with the corresponding $N_{\text{AE,max}}$ and is shown considering the logarithmic time scale in Fig. 7b. In the $\log(t)$—$N_{\text{AE}}/N_{\text{AE,max}}$—diagram, the normalised curves follow a similar trend for all single-stage creep phases, but a different trend for multi-stage creep phases. In general, the evolutions of N_{AE} and ε_a with time are similar.

The detected number of AE-events and the signal burst energy, evaluated in the following, are strongly dependent on the distance between the sensor and the source as well
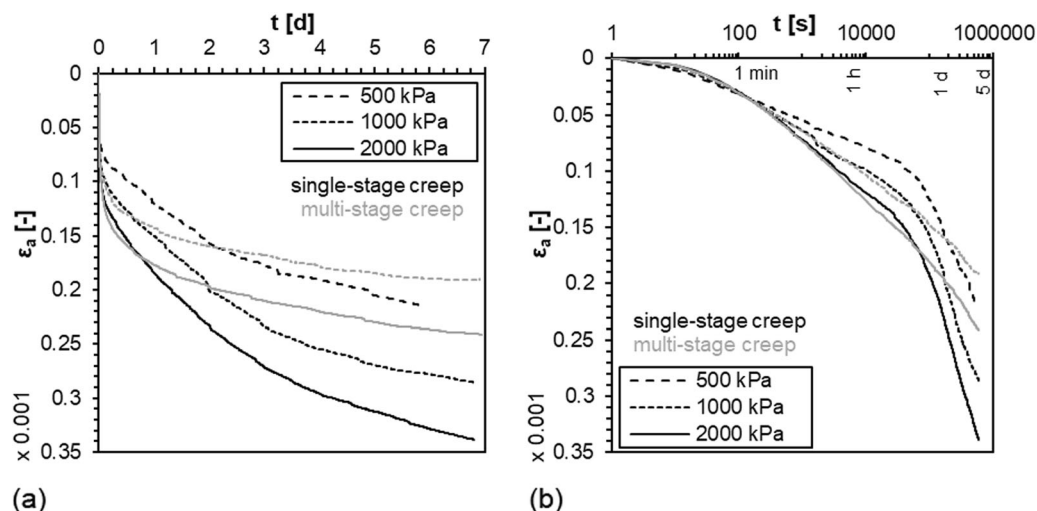

Fig. 5 Axial strain ε_a of single- and multi-stage creep phases at pressures of 500 kPa, 1000 kPa and 2000 kPa on dense to very dense samples of Cuxhaven sand in **a** linear and **b** logarithmic presentation
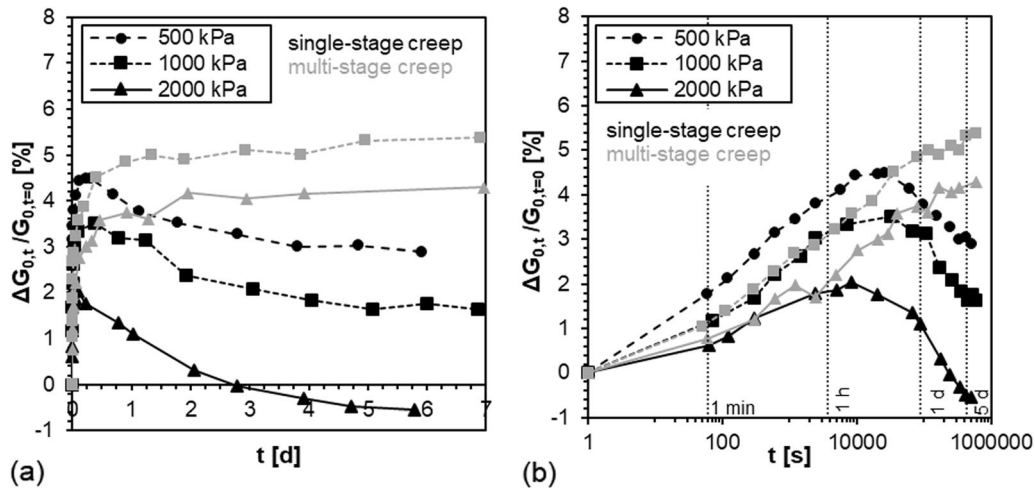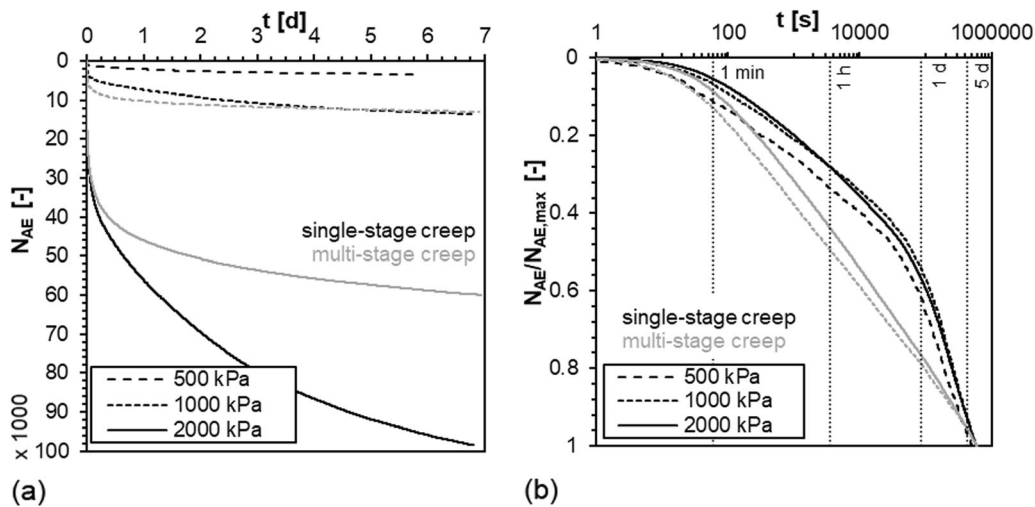
Fig. 6 Ageing $\Delta G_{0,t}/G_{0,t=0}$ of single- and multi-stage creep phases at pressures of 500 kPa, 1000 kPa and 2000 kPa on dense to very dense samples of Cuxhaven sand in **a** linear and **b** logarithmic presentation

Fig. 7 Evolution of **a** number of acoustic emissions N_{AE} with time and **b** normalised number of AE-events $N_{AE}/N_{AE,max}$ with $\log(t)$ of single- and multi-stage creep phases at pressures of 500 kPa, 1000 kPa and 2000 kPa on dense to very dense samples of Cuxhaven sand

as on the material damping. Therefore, the AE-sensors capture probably only a fraction of the AE-events occurring in the whole sample. For this reason, only a qualitative comparison of mechanical quantities (ε_a and $\Delta G_{0,t}/G_{0,t=0}$) with AE-quantities (N_{AE} and E) is possible.

In correspondence with N_{AE}, also the accumulated signal burst energy E increases significantly with increasing pressure. Thus, Fig. 8a shows E normalised to E_{max} with $\log(t)$. As can be seen, E evolves stepwise and the magnitude of the sudden energy releases varies during the time. In Fig. 8b, the number of AE-events (ordinate) exceeding a specific energy value E (abscise) is plotted in double logarithmic scale, as commonly assessed in the field of seismology to show the relationship between the number of seismic events and their magnitude which is proportional to the logarithm of the energy release during a seismic event.

As expected, events with low energy emissions (low magnitude) are more frequent than events with large energy emissions (large magnitude). The relationship between N_{AE} and E is approximately described by $\log(N_{AE}) = b - a \cdot \log(E)$ which follows the empirical Gutenberg–Richter's relationship between the number of seismic events N exceeding a given magnitude and the magnitude of earthquakes M. The intercept b is in general pressure- and history-dependent, while the inclination a shows minor dependence on pressure. In the multi-stage creep phases, a ranges from 0.96 to 1.16 and in the single-stage creep tests from 0.91 to 1.05, with the larger value of a at higher pressure. Restricted by the limitations of the AE measurement as previously mentioned, no general conclusion can be drawn; a possible dependence on pressure needs to be carefully analysed and further investigated.
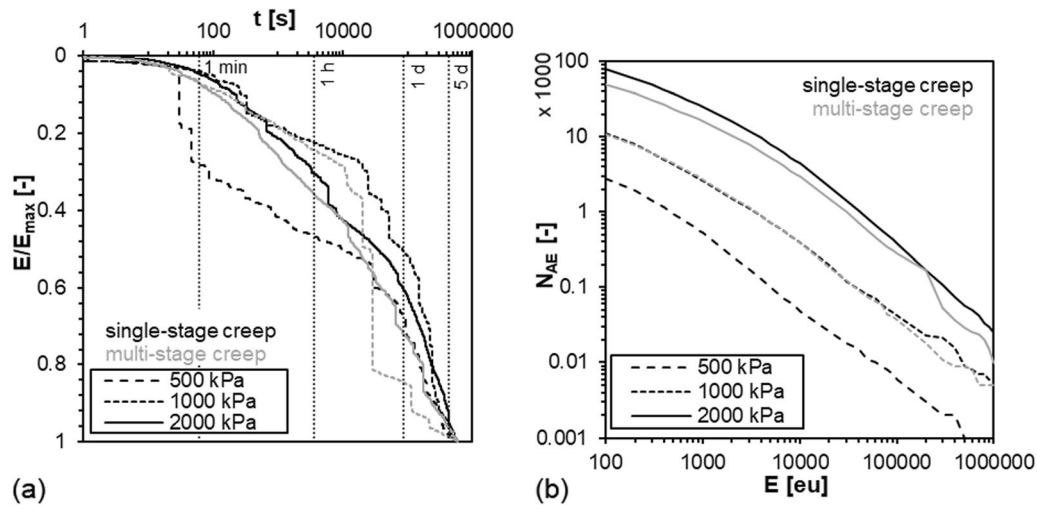
Fig. 8 **a** Normalised signal burst energy E/E_{max} versus $\log(t)$ and **b** number of AE-events N_{AE} exceeding E in double logarithmic presentation of single-stage and multi-stage creep phases at pressures of 500 kPa, 1000 kPa and 2000 kPa on dense to very dense samples of Cuxhaven sand

Regarding the dependence on the loading history, Fig. 8b shows that fewer AE-events occur in the multi-stage creep phase at 2000 kPa compared to the single-stage creep test. In the multi-stage creep test with 1000 kPa, a difference from the single-stage creep test can be observed for AE-events with $E > 40{,}000$ eu.

We assume that the energy releases are associated with the sudden conversion of potential in kinetic energy associated with instant sliding at the particle contact and particle motion. The larger the energy release, the larger the number of contacts where particles slide and the larger the redistribution of contact forces. Large energy releases can be associated with the rupture of force chains. A support for this explanation provides the evolution of axial strain rate $\dot{\varepsilon}_a$ and the change of the number of AE-events $\dot{N}_{AE}$ with time. Figure 9a shows $\dot{\varepsilon}_a$ for the single- and multi-stage creep tests as a function of time in a double logarithmic plot. The values of $\dot{N}_{AE}$ show a similar evolution with time as $\dot{\varepsilon}_a$ and are plotted in Fig. 9b. The relationship between the axial creep rate $\dot{\varepsilon}_a$, respectively, $\dot{N}_{AE}$ and the creep time t observed in the experiments can be described by Eq. (4).

$$\dot{\varepsilon}_a \left(or \dot{N}_{AE} \right) = t^{-m} \tag{4}$$

The exponent m slightly decreases with increasing pressure, e.g. $m = 0.93$ for $p\prime = 1000$ kPa and $m = 0.90$ for $p\prime = 2000$ kPa were determined for the evolution of $\dot{\varepsilon}_a$ in the multi-stage creep phases. The lower the pressure and hence the lower the forces at the particle contacts, the faster the particle assembly stabilises, and the smaller the creep strains. For the single-stage creep phases, a temporary quasi-stagnation, or for 500 kPa an increase of $\dot{\varepsilon}_a$, respectively $\dot{N}_{AE}$, is observed at about 10,000 s, which is associated with the rupture of strong force chains and

significant redistribution of forces towards a more stable structure. Stabilisation is indicated by $\dot{\varepsilon}_a$ (or $\dot{N}_{AE}$) approaching again a relation with the initial inclination m. As can be seen in Fig. 9b, the aforementioned stagnation is less abrupt for higher pressures and occurs at a higher rate.

In Fig. 9c, the normalised rates of change of the shear modulus $\dot{G}_{0,t}/G_{0,t=0}$ are shown whereas $\dot{G}_{0,t} \approx (G_{0,t} - G_{0,t=0})/\Delta t$. It is observed that $\dot{G}_{0,t}/G_{0,t=0}$ follows the same trend described by Eq. (4) for $\dot{\varepsilon}_a$ and $\dot{N}_{AE}$. The negative values of $\dot{G}_{0,t}/G_{0,t=0}$ observed during the single-stage creep tests, which are not plotted in the double logarithmic diagram, coincide with the stagnation of $\dot{\varepsilon}_a$, respectively $\dot{N}_{AE}$. It is interesting to note, that the exponents m for $\dot{N}_{AE}$ and $\dot{G}_{0,t}/G_{0,t=0}$ are similar to the exponent corresponding to the trend of $\dot{\varepsilon}_a$. In our opinion, this result confirms that creep and ageing are based on the same micromechanical processes.

In summary, the following conclusions can be drawn from the experimental investigations:

- Cuxhaven sand shows increasing axial creep strain with increasing isotropic pressure, whereas ageing increases with decreasing pressure.
- The time-dependent evolutions of the number of AE-events and axial creep strain follow the same trend.
- In the single-stage creep tests, an increase followed by a decrease of the shear modulus (ageing) is observed. The higher the pressure, the less pronounced is the initial increase of $\Delta G_{0,t}/G_{0,t=0}$ and more pronounced the subsequent decrease with time.
- The decrease of $\Delta G_{0,t}/G_{0,t=0}$ is accompanied by a temporary quasi-stagnation of the axial strain rate and the rate of number of AE-events $\dot{N}_{AE}$.
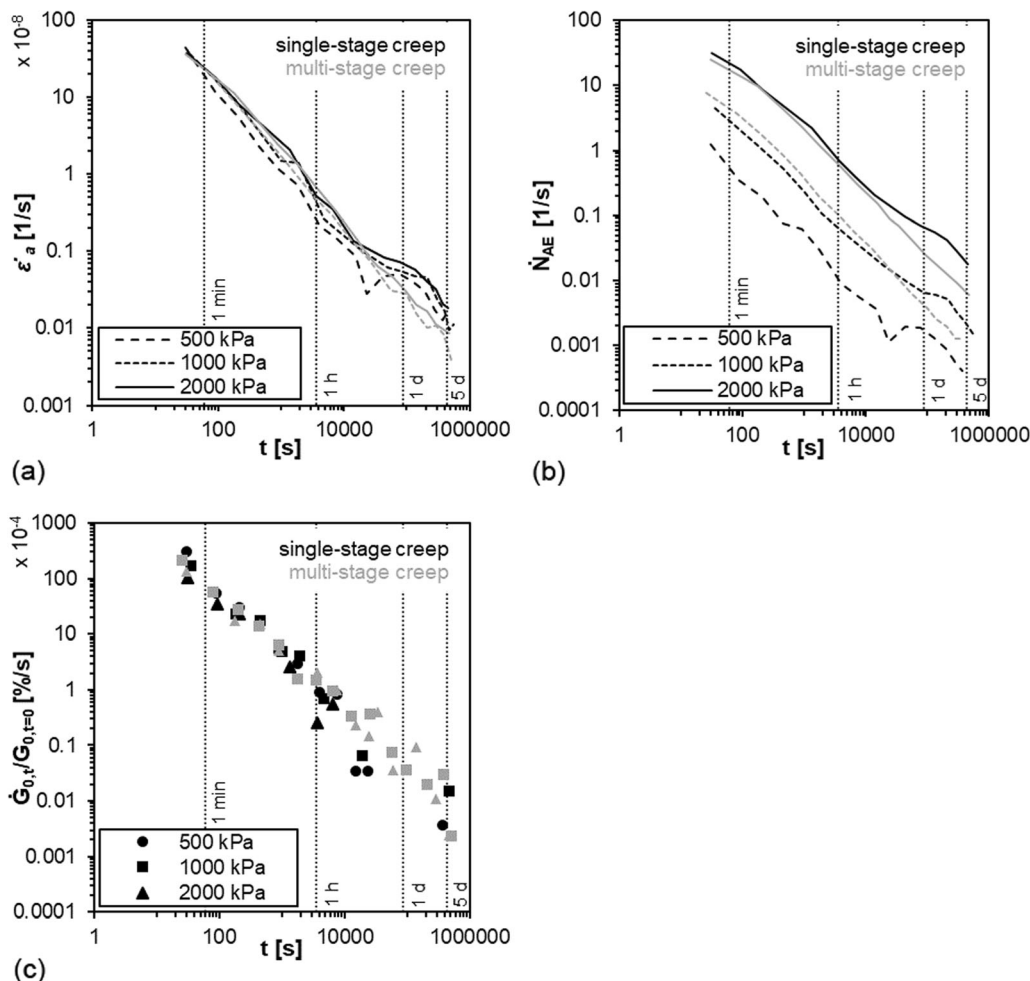
Fig. 9 **a** Axial strain rate $\dot{\varepsilon}_a$, **b** rate of number of AE-events $\dot{N}_{AE}$ and **c** rate of the normalised change of small-strain shear modulus $\Delta\dot{G}_{0,t}/G_{0,t=0}$ with time in double logarithmic presentation of single- and multi-stage creep phases at pressures of 500 kPa, 1000 kPa and 2000 kPa on dense to very dense samples of Cuxhaven sand

- Within the considered period of 5 days and for same isotropic pressure the multi-stage creep test shows less creep and therefore, more ageing than the single-stage creep tests.
- The stepwise evolution of the burst signal energy E indicates a dominant stick–slip mechanism at the particle contacts. The relationship between the number of AE-events N_{AE} exceeding a given energy threshold and the corresponding E is approximately linear in a double logarithmic scale. Thus, the Gutenberg-Richter law applies to micromechanical processes.
- Axial strain rate, rate of number of AE-events and the rate of change of small-strain shear modulus with time follow a power law.

Furthermore, the experimental results suggest that a time-dependent restructuring of the particle skeleton takes place, which will be subsequently described by a conceptual model.

4 Conceptual model

In the following, we present a conceptual model assuming a time-dependent behaviour of the normal and shear forces at the particle contacts to explain the experimental observations qualitatively. This conceptual model represents an attempt to unify our reflections with the descriptions of micromechanical processes found in the literature. The conceptual model is shown in Fig. 10.

As described by Yusa [41], the initial soil fabric plays a significant role in the evolution of ageing. For the presented experiments, ageing started after isotropic loading. It is shown that during isotropic compression the orientation of the particles becomes random [7, 37, 39]. Thus, at the onset of creep and ageing ($t = 0$ s) of particular single-stage creep tests, the fabric can be assumed to be more or less isotropic and unstructured. Hence, initially the force chains are evenly distributed but rather unstable and may redistribute randomly at a comparably high frequency
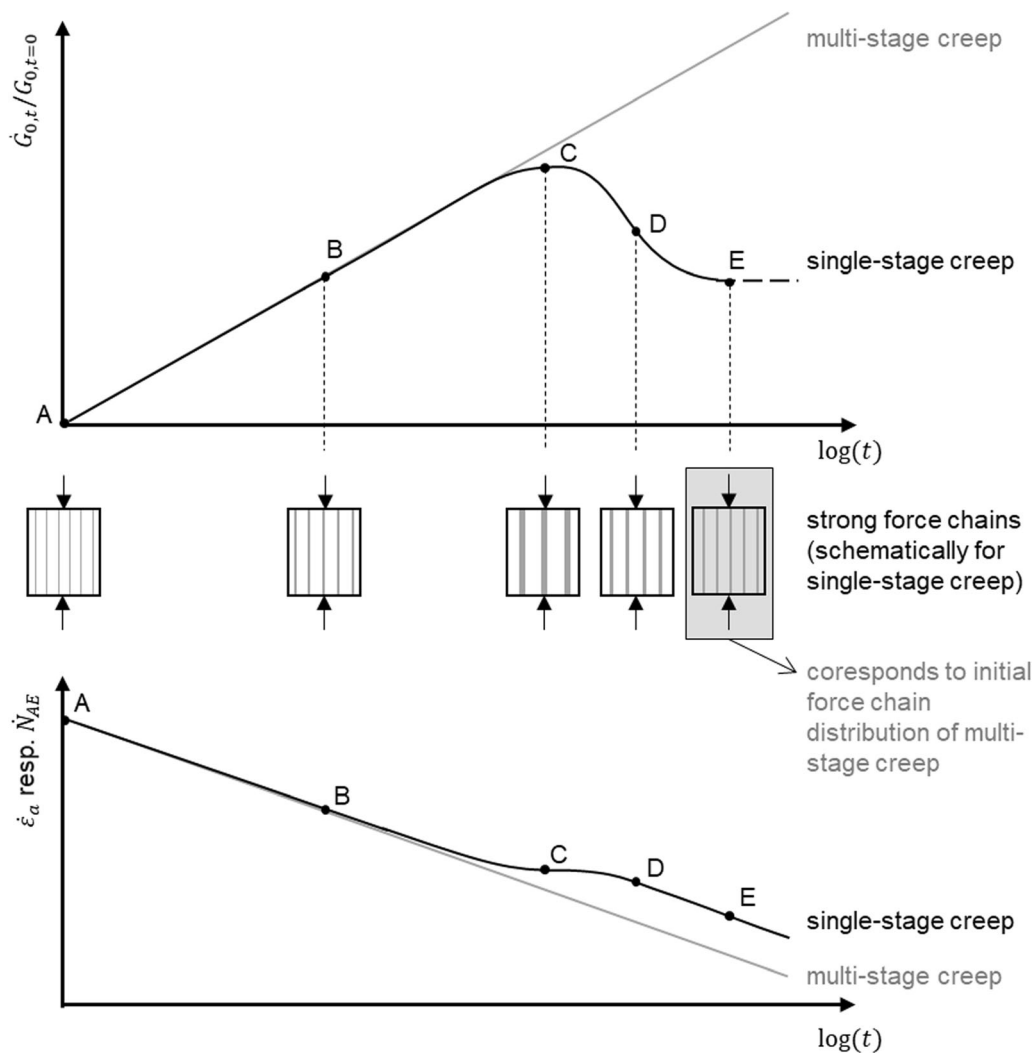
Fig. 10 Schematic representation of the conceptual model explaining creep and ageing behaviour in granular material; simplified to vertical loading direction, force chains other than in vertical direction are not depicted

(State A in Fig. 10). The vertical lines represent schematically force chains, which are carrying the pressure acting on the sample. For the sake of simplicity, only force chains in vertical direction are depicted. Obviously, force chains will develop in both vertical and horizontal direction during isotropic compression.

Initial instability of force chains results from the varying strength and stiffness at the contacts between particles. Each particle contact shows time-depended behaviour as a function of the magnitude of the transferred shear and normal force. Creep rupture at the particle scale may occur at loadings close to the breakage of small particle asperities changing the particle morphology and surface texture. Under high loads, extensive particle breakage may happen. The weakest contacts fail or at least change at a faster rate during loading as well at the start of a creep phase. A more pronounced initial instability of the force chains and the resulting rearrangement of particles causes the creep rate to

show the largest value at the beginning of a creep phase. With increasing time during creep, the particles cluster and interlock [7]. In comparison with the initial state, contact forces concentrate in fewer, but the comparably stiffer "strong" force chains (State B in Fig. 10). The normal and the tangential contact forces carried by particle clusters within the strong force chain increase, whereas they decrease in the "weak" cluster. The stronger and localized the force chains, the initially stiffer the assembly of particles is. Following this, the number of sliding contacts tends towards a minimum and the creep rate decreases. Nonetheless, due to delayed breakage such as creep failure or limited plastic effects corresponding to softening at the contact, stiffness of strong force chains is not permanent. An abrupt de-stabilisation of the concentrated force chains may occur when some of the strongly loaded contacts within the force chain fail, possibly causing a chain reaction, through which the condition of several contacts

changes from stick to slip at almost the same time. The state C is interpreted as the onset of de-stabilisation of the strong force chains. This state corresponds to the maximum value of $\Delta G_{0,t}/G_{0,t=0}$ within the observation time and the maximum fluctuation of contact forces. Abrupt contact slip and particle rearrangement are connected with a discrete release of kinetic energy. The detected jumps in the signal burst energy E (Fig. 8a) indicate that abrupt energy releases actually happen during creep. However, because of the limitations of the conducted AE-measurements mentioned in chapter 3, in our experiments, we are not able to capture the energy conversion occurring exactly at point C.

The collapse of the strong force chains leads to a contact force redistribution from the previously strong to the previously weak particle clusters. The temporary de-stabilisation of the particle assembly at state C causes the non-permanent stagnation of the creep rate observed in the experiments. The process of regaining stiffness that may be associated with a process of re-stabilisation from C to E takes a comparably long time in contrast to the initial stabilisation. These differences regarding the rate of increasing stiffness may be associated with secondary collapse effects, which are comparable to aftershocks occurring days and weeks after strong earthquakes. We presume that during the re-stabilisation, the structure evolves towards a more homogeneous force distribution in comparison with state C. Macroscopically, the different rates at which stiffness increases are indicated by the changing exponent m in Eq. (4) describing the time-evolution of $\dot{\varepsilon}_a$ and $\dot{N}_{AE}$, respectively, towards its initial value.

During the multi-stage creep phases, the initial fabric and force chain distribution result from loading history including previous creep at a lower pressure level (State E in Fig. 10). Assuming that the duration of previous creep phases is long enough to induce de-stabilisation, the initial structure at the beginning of the multi-stage creep phases is more stable than at the start of a corresponding single-stage creep test. Thus, the monotonic increase of the shear modulus at small strain observed for the multi-stage creep phases results from a previously more intense homogenisation process of force chains.

5 Concluding remarks

We conducted a combined study of ageing and creep of dry, dense samples of silica sand using triaxial apparatus. From isotropic loading paths, we conclude that there is an inversely proportional relationship between creep and ageing. From increasing contact sliding and particle motion, leading to creep, follows a variation in the pattern of strongly loaded force chains, which are linked to a

relative decrease in ageing rate. Different intensities of recorded acoustic emissions indicate that the processes can be traced back to changes in the force chains driven by different degrees of particle breakage and particle motion.

In single-stage creep tests, a non-permanent formation followed by delayed collapse of strong force chains induced by the failure of highly loaded particle contacts is proposed. In the multi-stage creep tests the force chains within the particle assembly developed in the preceding creep phase are already comparably stable. Accordingly, the development of structure as a pattern of force chains within the particle assembly depends not only on the isotropic pressure but moreover on the loading history.

It is likely that the ageing behaviour of young deposits of granular material can be described according to the experimental findings and the conceptual model proposing a time-dependent homogenisation process of force chains.

Finally, the findings of our experimental investigations, especially the development of the measured quantities expressing creep and ageing $G_{0,t}$, ε_a, N_{AE} and E, respectively, as well as their time derivatives provide an experimental database for the development, validation and calibration of advanced contact models. In contrast to continuum mechanics, such contact models are required to simulate the time-dependent behaviour of granular material with respect to the different scales of observation. The discrete element method (DEM) may provide a better insight to the time-dependent mechanics of individual particle contacts and changing force chains in granular assemblies.

Data availability The datasets generated during and/or analysed during the current study are available from the corresponding author on reasonable request.

Declarations

Conflict of interest The authors have no relevant financial or non-financial interests to disclose.

References

1. Afifi SS, Woods RD (1971) Long-Term pressure effects on shear modulus of soils. J Soil Mech Found Div 97(10):1445–1460

2. Anderson DG, Stokoe KH (1978) Shear modulus: a time-dependent soil property. In: Ebelhar RJ (ed) Dynamic geotechnical testing. ASTM International, West Conshohocken

3. Augustesen A, Liingaard M, Lade PV (2004) Evaluation of time-dependent behavior of soils. Int J Geomech 4(3):137–156. https://doi.org/10.1061/(ASCE)1532-3641(2004)4:3(137)

4. Baxter CDP, Mitchell JK (2004) experimental study on the aging of sands. J Geotech Geoenviron Eng 130(10):1051–1062. https://doi.org/10.1061/(ASCE)1090-0241(2004)130:10(1051)

5. Bock BA-M, Levin F, Vogt S et al (2022) Acoustic emission of sand during creep under Oedometric compression. Geotech Test J 45(2):20210007. https://doi.org/10.1520/GTJ20210007

6. Bock BA-M, Vogt S, Cudmani R (2021) Zeitabhängige Änderung des Schubmoduls bei kleinen Scherdehnungen in granularen Materialien. In: Proceedings of the 3. Bodenmechanik Tagung, online

7. Bowman ET, Soga K (2003) Creep, ageing and microstructural change in dense granular materials. Soils Found 43(4):107–117. https://doi.org/10.3208/sandf.43.4_107

8. Carroll R, Carotenuto P, Dano C et al (2020) Field experiments at three sites to investigate the effects of age on steel piles driven in sand. Géotechnique 70(6):469–489. https://doi.org/10.1680/jgeot.17.P.185

9. Charles-Cruz CA, Cousens TW, Stewart DI (2008) Compressibility and Creep Behaviour of Hydraulically Placed PFA and Mine Tailings Fills. In: Paper presented at the 12th international conference of international association for computer methods and advances in geomechanics (IACMAG), Goa

10. Chow FC, Jardine RJ, Nauroy JF et al (1997) Time-related increases in the shaft capacities of driven piles in sand. Tech Note Géotech 47(2):353–361

11. Cudmani R, Jörger R, Wolski K (2011) Sydney, hafenerweiterung port botany: wirtschaftliche lösungen für höchste geotechnische anforderungen. Technische Universität Berlin, Berlin

12. Gao Y, Wang Y-H, Su JCP (2013) Mechanisms of aging-induced modulus changes in sand under isotropic and anisotropic loading. J Geotech Geoenviron Eng 139(3):470–482. https://doi.org/10.1061/(ASCE)GT.1943-5606.0000772

13. Deutsches Institut für Normung e.V. (DIN) (2012) Geometrische Produktspezifikation (GPS) - Oberflächenbeschaffenheit: Flächenhaft—Teil 2: Begriffe und Oberflächen-Kenngrößen DIN EN ISO 25178–2:2012. Accessed 03 Jun 2021

14. Karimpour H, Lade PV (2010) Time effects relate to crushing in sand. J Geotech Geoenviron Eng 136(9):1209–1219. https://doi.org/10.1061/(ASCE)GT.1943-5606.0000335

15. Koerner RM, Lord AE, McCabe WM et al (1976) Acoustic emission behavior of granular soils. J Geotech Eng Div 102(GT7):761–774

16. Koerner RM, McCabe WM, Lord AE (1981) Acoustic emission behavior and monitoring of soils. In: Drnevich VP, Gray RE (eds) Acoustic emissions in geotechnical engineering practice, ASTM STP 750. ASTM, West Conshohocken, pp 93–141

17. Krumbein W, Sloss LL (1963) Stratigraphy and sedimentation. In: A series of books in geology. Freeman, San Francisco

18. Kuhn MR, Mitchell JK (1993) New perspectives on soil creep. J Geotech Eng 119(3):507–524. https://doi.org/10.1061/(ASCE)0733-9410(1993)119:3(507)

19. Kuwano R, Jardine RJ (2002) On measuring creep behaviour in granular materials through triaxial testing. Can Geotech J 39(5):1061–1074. https://doi.org/10.1139/t02-059

20. Lade PV, Liggio CD, Nam J (2009) Strain rate, creep, and stress drop-creep experiments on crushed coral sand. J Geotech Geoenviron Eng 135(7):941–953. https://doi.org/10.1061/(ASCE)GT.1943-5606.0000067

21. Lade PV, Liu C-T (1998) Experimental study of drained creep behavior of sand. J Eng Mech 124(8):912–920. https://doi.org/10.1061/(ASCE)0733-9399(1998)124:8(912)

22. Levin F, Vogt S (2015) Creep of Sand in Filled Open Cast Mining Pits. In: Dijkstra, J., Karstunen et al. (eds) Proceedings of the International Conference on Creep and Deformation Characteristics in Geomaterials. Chalmers University of Technology, Gothenburg, Sweden

23. Mesri G, Feng TW, Benak JM (1990) Postdensification penetration resistance of clean sands. J Geotech Eng 116(7):1095–1115. https://doi.org/10.1061/(ASCE)0733-9410(1990)116:7(1095)

24. Mesri G, Vardhanabhuti B (2009) Compression of granular materials. Can Geotech J 46(4):369–392. https://doi.org/10.1139/T08-123

25. Michalowski RL, Wang Z, Nadukuru SS (2018) Maturing of contacts and ageing of silica sand. Géotechnique 68(2):133–145. https://doi.org/10.1680/jgeot.18.D.004

26. Mitchell JK (2005) Fundamentals of soil behavior, 3rd edn. John Wiley & Sons, Hoboken

27. Mitchell JK, Solymar ZV (1984) Time-dependent strength gain in freshly deposited or densified sand. J Geotech Eng 110(11):1589–1576

28. Miura S, Toki S (1982) Sample preparation method and its effect on static and cyclic deformation—strength properties of sand. Soils Found 22(1):61–77

29. Murayama S, Michihiro K, Sakagami T (1984) Creep characteristics of sands. Soils Found 24(2):1–15. https://doi.org/10.3208/sandf1972.24.2_1

30. Naderi-Boldaji M, Bahrami M, Keller T et al (2017) Characteristics of acoustic emissions from soil subjected to confined uniaxial compression. Vadose Zone J. https://doi.org/10.2136/vzj2017.02.0049

31. Radjai F, Wolf DE, Jean M et al (1998) Bimodal character of stress transmission in granular packings. Am Phys Soc 80(1):61–65

32. Schmertmann JH (1991) The mechanical aging of soils. J Geotech Eng 117(9):1288–1330. https://doi.org/10.1061/(ASCE)0733-9410(1991)117:9(1288)

33. Shiotani T, Ohtsu M (1999) Prediction of slope failure based on AE activity. In: Vahaviolos SJ (ed) Acoustic emission: standards and technology update. ASTM, West Conshohocken

34. Skov R, Denver H (1988) Time-dependence of bearing capacity of piles. In: Proceedings of 3rd International Conference on the application of stress-wave theory to piles, pp 879–888

35. Smith A, Dixon N (2019) Acoustic emission behaviour of dense sands. Géotechnique 69(12):1107–1122. https://doi.org/10.1680/jgeot.18.P.209

36. Smith A, Dixon N, Meldrum P et al (2014) Acoustic emission monitoring of a soil slope: comparisons with continuous deformation measurements. Géotech Lett 4(4):255–261. https://doi.org/10.1680/geolett.14.00053

37. Thornton C, Barnes DJ (1986) Computer simulated deformation of compact granular assemblies. Acta Mech 64(1–2):45–61. https://doi.org/10.1007/BF01180097

38. Vaid YP, Negussey D (1984) Relative density of pluviated sand samples. Soils Found 24(2):101–105. https://doi.org/10.3208/sandf1972.24.2_101

39. Wiebicke M, Herle I, Andò E et al (2020) Measuring the fabric evolution of sand—application and challenges. geotechnik 44(2):114–122. https://doi.org/10.1002/gete.202000019

40. Ye J, Haiyilati Y, Cao M et al (2022) Creep characteristics of calcareous coral sand in the South China Sea. Acta Geotech 17(11):5133–5155. https://doi.org/10.1007/s11440-022-01634-1

41. Yusa M (2015) Aging and creep of non-plastic silty sand. Dissertation, University of Canterbury